The Impacts of Image Resolution on Permeability Simulation of Gas Diffusion Layer Using Lattice Boltzmann Method

F. Jinuntuya[a], R. Chen[a], H. Ostadi[b], K. Jiang[b], Y. Gao[c], X. Zhang[c]

[a] Department of Aeronautical and Automotive Engineering,
Loughborough University, Leicestershire LE11 3TU, UK
[b] Centre for Bio-medical and Micro Engineering, School of Mechanical Engineering,
University of Birmingham, Birmingham B15 2TT, UK
[c] Department of Engineering, University of Liverpool, Liverpool L69 3GH, UK

The effect of image resolution on gas permeability through the x-ray reconstructed carbon paper gas diffusion layer (GDL) of a polymer electrolyte fuel cell (PEFC) was examined in this paper. The 3D models of the GDL at 6 different resolutions were obtained by the x-ray computed tomography imaging technique. Each GDL image was then characterized its gas permeability through the lattice Boltzmann (LB) numerical method. The results suggest that the image resolution has a great impact on gas permeability in both principal and off-principal flow directions. The coarser resolutions can contribute to significant changes in the resulting permeability. However, it can reduce calculation time to a great extent. The results also indicate that the GDL image at the resolution of 2.72 μm provides a good compromise between computation time and accuracy.

Introduction

Gas diffusion layer plays an important role in the overall performance and durability of a PEFC by serving several functions including providing pathways for reactant gases to access the reaction sites; product water removal; heat and electronic transport and also serving as a mechanical support for the membrane. The GDL is a heterogeneous porous carbon-based material typically made of woven carbon cloth or non-woven carbon paper with thickness and mean pore diameter in the order of 100 μm and 10 μm, respectively (1). To date, experimental measurements of fluid flows and associated parameters in the diminutive structure of the GDL remain difficult. Therefore, numerical models have been extensively developed and applied to examine fluid transport through the GDL.

Among various approaches, the particle-based LB method has been increasingly utilized to investigate fluid transport behaviors in porous materials. Unlike the conventional CFD method, where the incorporation of boundary-fitted grid in complicated solid boundaries of the GDL is extremely difficult, the LB method has the capability to implement boundary conditions in such complex geometries by imposing the bounce-back scheme to the fluid particle distribution (2). A number of studies have been conducted using LB method to examine complex flows through carbon paper and carbon cloth GDL structures at pore-scale (3-6). However, those works employed the virtual stochastic generation method which is based on specified statistic information of a

GDL sample to create the representative models for flow simulation (7). Though this approach is relatively more rapid and less expensive than generating the GDL model through the experimental imaging technique, it does not closely represent microscopic features of the actual GDL as manufactured (8-9).

In order to accurately reflect the actual GDL structure, the x-ray computed tomography reconstruction technique has been used to generate 3D representative structures of GDL samples. The combination of the two advanced techniques has also been successfully applied to study fluid movement through PEFC GDLs in recent publications (8-13). However, the high computational demand of the LB method together with using the highest available resolution of the x-ray images has limited its application to analyze only a very small volume of the GDL. With such high resolutions, the LB flow simulation is also extremely time-consuming.

In this work, the effect of image resolution on gas permeability through the x-ray reconstructed GDL was examined by using the LB method. The binary 3D models of the GDL at 6 different resolutions were acquired by using the x-ray imaging technique. Each image was then integrated into a single-phase LB numerical solver to characterize its gas permeability. The resulting permeability, its sensitivity to the resolution variation and the computational time were analyzed to identify the optimum resolution for the representative model of the GDL.

Methodology, Results and Discussion

Lattice Boltzmann method

In this study, the three-dimensional single-time relaxation LB model was used to simulate gas flow through the GDL. Principally, the LB method tracks the movements and collisions of a number of fictitious fluid particles in a lattice domain. The movement of each fictitious particle is described by the particle distribution function $f_i(x,t)$ which defines the mass of a particle at location x and time t moving with the velocity ξ_i along the direction i

$$f_i(x+\xi_i\delta t, t+\delta t) = f_i(x,t) + \frac{1}{\tau}\left[f_i^{eq}(x,t) - f_i(x,t)\right] \qquad [1]$$

where $f_i^{eq}(x,t)$ is the equilibrium distribution function and τ is the dimensionless relaxation parameter that controls the rate at which $f_i(x,t)$ approaches $f_i^{eq}(x,t)$. The equilibrium distribution function $f_i^{eq}(x,t)$ is given by

$$f_i^{eq}(x,t) = w_i\left\{\rho + \rho_0\left[\frac{\xi_i \cdot u}{c_s^2} + \frac{1}{2}\left(\frac{\xi_i \cdot u}{c_s^2}\right)^2 - \frac{u \cdot u}{2c_s^2}\right]\right\} \qquad [2]$$

where w_i is a weighting factor depending on the magnitude of the velocity ξ_i, c_s is the speed of sound. The bulk fluid density ρ and velocity u are obtained by summing the corresponding distribution functions of all incoming particles at each node in the lattice domain as follows

$$\rho = \sum_i f_i = \sum_i f_i^{eq} \quad [3]$$

$$\rho_0 u = \sum_i f_i \xi_i = \sum_i f_i^{eq} \xi_i \quad [4]$$

where ρ_0 is a reference density and assumed to equal unity.

The D3Q19 LB scheme was employed in this work where fluid particles in each lattice node are able to move in 19 directions from the origin in the 3-dimensional regime as shown in Figure 1.

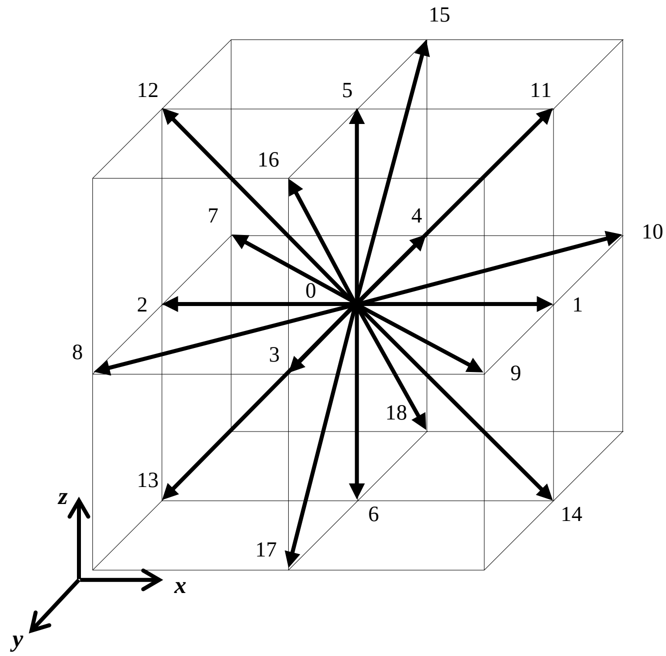

Figure 1. The 19 velocity directions in the D3Q19 LB scheme.

The LB implementation involves a collision step and a streaming step. In a collision step, the term on the right-hand side of Eq.[1] is calculated as $f_i^*(x,t) = f_i(x,t) + \left[f_i^{eq}(\rho,u) - f_i(x,t) \right] / \tau$. The streaming step moves the outcomes of collisions $f_i^*(x,t)$ from the location x to the nearest location $x + \delta t \xi_i$ along their direction of motion at time $t + \delta t$ to become $f_i(x + \delta t \xi_i, t + \delta t) = f_i^*(x,t)$. After the streaming step has been completed, the gas density ρ and velocity u for each node in the lattice domain are then updated through $\rho(x, t+\delta t) = \sum_i f(x, t+\delta t)$ and $\rho_0 u = \sum_i f_i(x, t+\delta t)$, respectively (10).

In the LB model, the bounce-back scheme for no-slip boundaries is used to solve fluid-solid boundary conditions by assuming that any fluid particle that hits a solid boundary during the streaming step is simply bounced back to its original position at the end of each time step. To drive gas flow, a pressure difference is applied to two opposite sides of the domain in one direction while the other four sides are treated as periodic boundaries where the particles exiting of the domain from one side re-enter the domain through its opposite side (10).

Permeability calculation

The detailed gas velocity distribution in the GDL domain at the microscopic scale obtained from the LB simulation is used to calculate the absolute permeability at the macroscopic scale. The absolute permeability of the GDL *k* is defined by Darcy's law as

$$k = \frac{\rho \mu q}{\left(\Delta P / L\right)} \qquad [5]$$

where ρ is the gas density, q is the average gas velocity through the GDL in the direction of the pressure gradient, ΔP is the applied pressure gradient across the GDL domain, L is the size of the domain and μ is the dynamic viscosity which is related to the dimensionless relaxation time as

$$\mu = \delta x^2 \left(\tau - 0.5\right) / 3\delta t \qquad [6]$$

By applying a pressure difference in the through-plane direction (z-direction), gas can also flow in the in-plane direction (y- and x- directions). The three components of permeability tensor in principal and off-principal flow directions can be calculated as

$$k_{zz} = \frac{\rho \mu q_z}{\left(\Delta P / L_z\right)};\ k_{yz} = \frac{\rho \mu q_y}{\left(\Delta P / L_z\right)};\ k_{xz} = \frac{\rho \mu q_x}{\left(\Delta P / L_z\right)} \qquad [7]$$

where q_x, q_y, q_z are the average velocities and L_x, L_y, L_z are the sizes of the domain in x-, y- and z-directions, respectively. The average velocities in the three directions are

$$q_x = \frac{\sum_i u_x\left(x_i\right)}{L_x L_y L_z};\ q_y = \frac{\sum_i u_y\left(x_i\right)}{L_x L_y L_z};\ q_z = \frac{\sum_i u_z\left(x_i\right)}{L_x L_y L_z} \qquad [8]$$

Digital 3D model

In this current study, the digital image of a carbon paper GDL sample was originally generated at the resolution of 0.68 μm/pixel through the x-ray computed tomography imaging technique. In general, there are three key steps to generate the 3D images including progressive 2D imaging using x-ray tomography, image processing, and digital 3D reconstruction. The details of image acquisition and reconstruction of the GDL were reported in Ref. 10 and 14.

In order to examine the pixel size effect on the absolute permeability, a number of 3D images were then further generated based on the original resolution starting with 2 times up to 6 times larger than the original pixel size. Therefore, the GDL images with the resolution of 0.68, 1.36, 2.04, 2.72, 3.40, and 4.08 μm/pixel, respectively were employed to study the impact on the resulting permeability. The 3D and 2D image of the reconstructed GDL sample with the size of 211 μm × 204 μm × 224 μm including domain division into 4 regions are illustrated in Figure 2 and 3, respectively. Figure 4 compares the 3D images with 6 different resolutions of region 1 in the sample. The size of each region in voxels and physical dimensions for each resolution are shown in Table I.

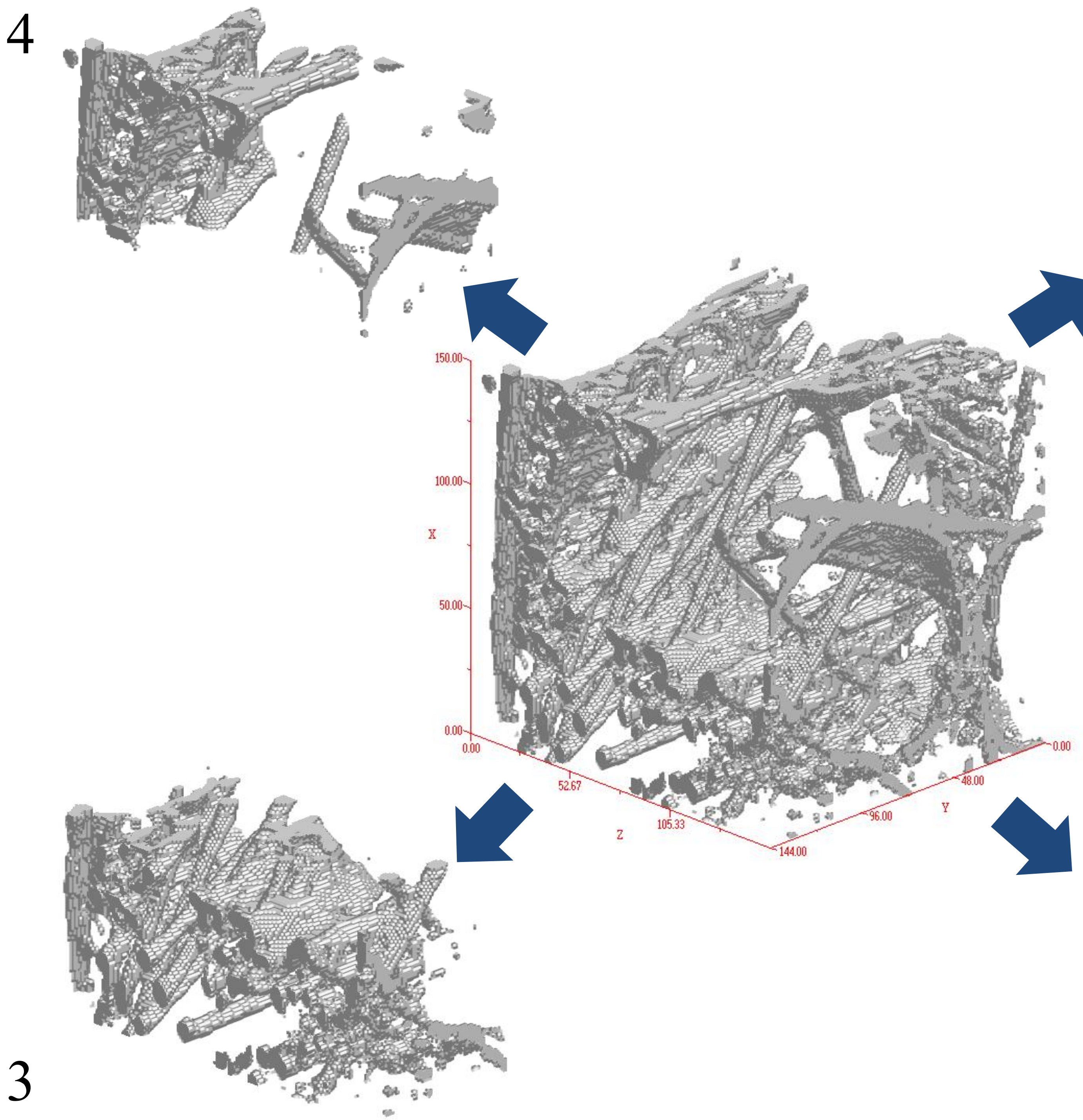

Figure 2. 3D image of the GDL sample with domain division into 4 regions.

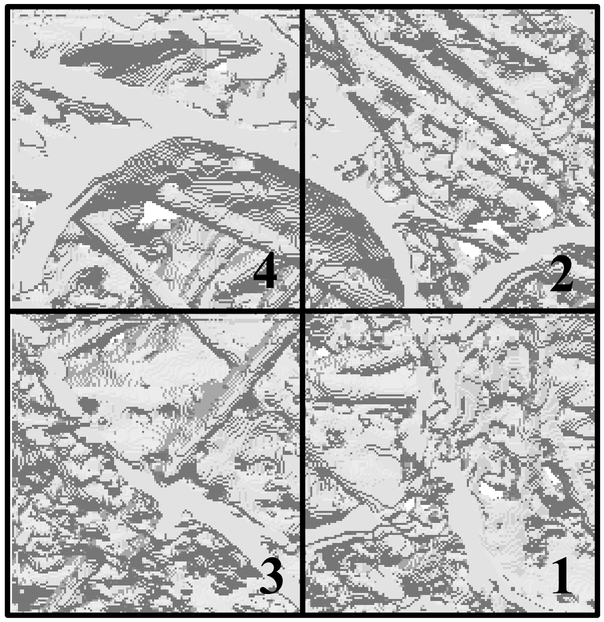

Figure 3. 2D image of the GDL sample with 4 regions of interest.

TABLE I. Image size for each region of the 3D GDL image with 6 different resolutions.

Resolutions	Image size in voxels			Image size in μm		
(μm/pixel)	x	y	z	x	y	z
0.68	155	150	329	105.40	102.00	223.72
1.36	78	75	164	106.08	102.00	223.04
2.04	52	50	109	106.08	102.00	222.36
2.72	39	38	82	106.08	103.36	223.04
3.40	31	30	65	105.40	102.00	221.00
4.08	26	25	54	106.08	102.00	220.32

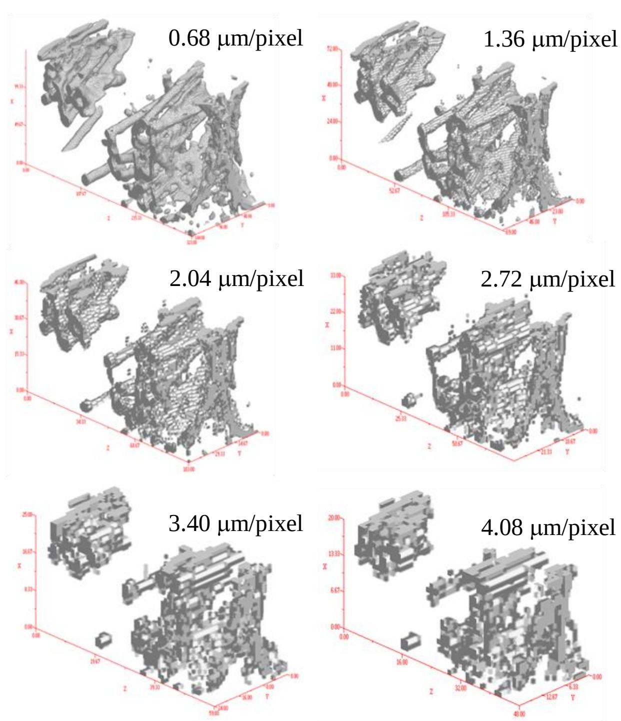

Figure 4. 3D images of region 1 with 6 different resolutions including 0.68, 1.36, 2.04, 2.72, 3.40 and 4.08 μm/pixel, respectively.

Simulated permeability

The single-phase LB model with the D3Q19 scheme was applied to each of the 4 regions of the GDL images reconstructed with the 6 different resolutions including 0.68, 1.36, 2.04, 2.72, 3.40 and 4.08 μm/pixel. To simulate gas flow through the GDL, the pressure difference of 10 Pa was applied to each region and the entire void space was assumed to be filled with air. The principal flow direction was set in the through-plane direction along the GDL thickness. The detailed gas velocity field obtained from the LB simulation was then used to predict the gas permeability through the simulated GDL domain by using Darcy's law. All simulations were carried out on a quad-core 2.33 GHz workstation with 3.25 GB RAM.

Figure 5(a)-(c) illustrate the simulated permeability in the principal through-plane flow direction (z-direction) and the off-principle in-plane flow directions (y- and x-directions) when the pressure gradient is applied in the through-plane direction. According to Figure 5(a)-(c), the gas permeability in all flow directions varies locally among each simulated region thus the means are chosen as the representative values for all regions. The mean simulated values of the gas permeability both in principal through-plane and off-principal in-plane flow directions, and the average calculation time for each of 6 resolutions are given in Table II.

The results indicate that the variation of the image resolution contributes to a great difference on the predicting permeability in all flow directions. Assuming that the GDL image reconstructed by the original resolution of 0.68 μm provides the most accurate set of permeability values, all sets of results over the range of resolutions show that the differences are up to 30%, 32% and 26% for the resulting through-plane permeability and in-plane permeability in y- and x-directions, respectively as illustrated in Figure 6. For the through-plane direction, the lowest resolution of 4.08 μm gives a largest difference in the resulting permeability as in the x-direction while the 3.40 μm resolution causes the greatest increase in permeability in the y-direction. On the other hand, these two coarsest resolutions lead to a massive reduction in terms of computational time from approximately 1620 minutes per each region of the original resolution to just about 1 minute as shown in Table II.

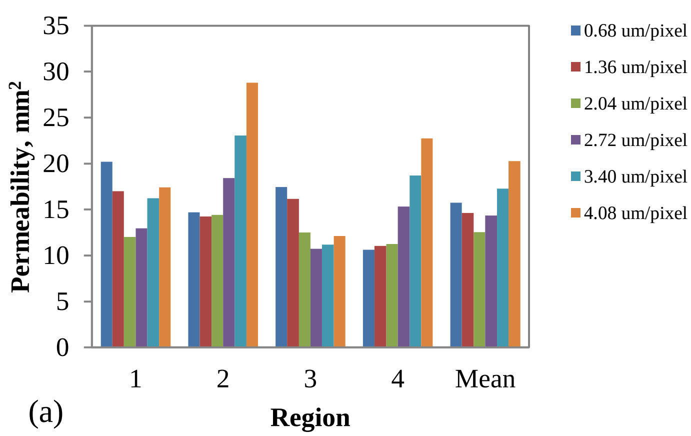

(a)

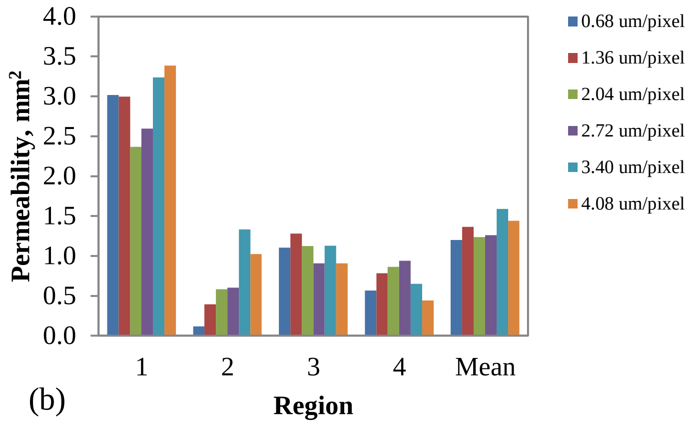

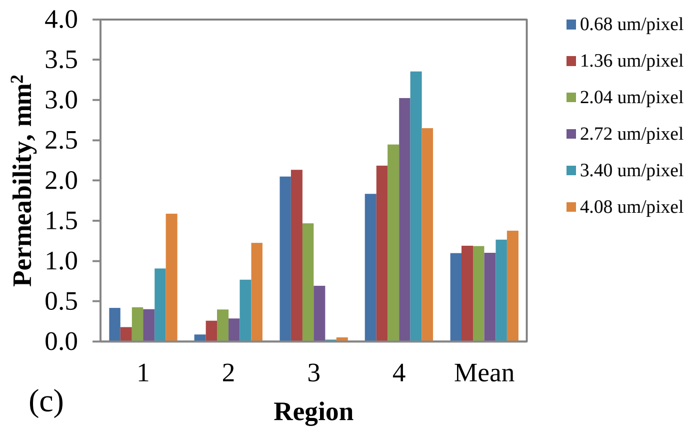

Figure 5. Simulated absolute permeability in (a) through-plane direction (z-direction); (b) in-plane y-direction; (c) in-plane x-direction; for the 4 regions with 6 different resolutions including the mean values.

Figure 6 also illustrates that the 1.36 μm image resolution produces the least difference of 7.1% from the original resolution for the through-plane permeability as expected. However, the image resolution of 2.04 and 2.72 μm offer the more accurate results with only 2.8% and 0.3% difference for the in-plane y- and x-directions, respectively while the differences are more than 13% and 8%, respectively for the case of 1.36 μm resolution. This therefore demonstrates that the higher resolution does not always provide the more accurate results than the lower resolutions.

The results also indicate that the GDL image at the resolution of 2.72 μm presents a good compromise between accuracy and simulation time. The resulting permeability values are less than 8%, 5% and 0.3% difference for the through-plane direction and in-plane in y- and x-directions, respectively while the calculation time reduces greatly to just 4 minutes which is approximately 400 times less than the original resolution. By utilizing the 2.72 μm resolution, simulations are also able to analyze the gas flow characteristics in a 64 times larger in terms of domain size.

TABLE II. Mean simulated through-plane permeability, in-plane permeability in y- and x-directions and mean calculation time in each region of the reconstructed GDL sample at 6 different resolutions**.**

Resolutions (μm/pixel)	Mean through-plane permeability	Mean in-plane permeability	Mean in-plane permeability	Mean Calculation

	(mm^2)	y-direction (mm^2)	x-direction (mm^2)	time (min)
0.68	15.7332	1.2022	1.0981	1620
1.36	14.6168	1.3642	1.1893	63
2.04	12.5515	1.2353	1.1845	10
2.72	14.3591	1.2612	1.1006	4
3.40	17.2916	1.5874	1.2636	1
4.08	20.2754	1.4397	1.3783	<1

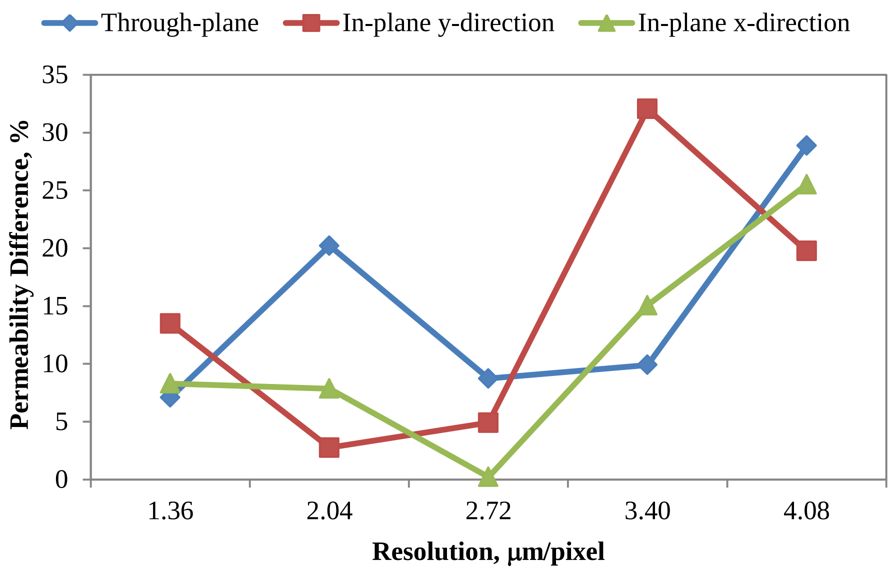

Figure 6. Percentage difference on the mean permeability in the through-plane direction and in-plane in y- and x-directions of the GDL images at resolutions of interest, comparing with the 0.68 μm resolution image.

Conclusions

This study was conducted using the LB method and the x-ray computed tomography technique. The 3D models of the GDL at 6 different resolutions were generated via the x-ray reconstruction technique. Each of the images was then incorporated into the LB solver to predict its permeability. The effect of image resolution on gas permeability through the representative models of the actual GDL was studied. It was found that the resolution variation has a great impact on the resulting permeability in both principal and off-principal flow directions. The coarser resolutions contribute to significant changes in resulting mean permeability up to 30% and 32% for the principal and off-principal flow directions, respectively. Conversely, the average calculation time reduces greatly from 27 hours to less than 1 minute over the range of resolutions. The results also suggest that the GDL image at the resolution of 2.72 μm, a 4 times larger than the original resolution, gives a good compromise for permeability simulation in which around 400 times less in computation time and less than 8% difference in permeability can be obtained. In addition, with this resolution it is possible to investigate gas flows in a 64 times larger domain. In conclusion, it is worth considering the effect of image resolution to identify the optimum resolution for the representative GDL model which potentially improve computational efficiency in terms of simulation time reduction then substantially lowering computational costs or even allow simulation in a greater GDL volume while the accuracy is still satisfactory.

References

1. M. F. Mathias, J. Roth, J. Fleming and W. Lehnert, in *Handbook of Fuel Cells – Fundamentals, Technology and Applications*, vol.3, W. Vielstich, H. A. Gasteiger and A. Lamm, Editors, p. 517–537, John Wiley & Sons, New York (2003).
2. J. Zhang, *Microfluid Nanofluid*, **10**, 1 (2011).
3. J. Park, M. Matsubara and X. Li, *J. Power Sources*, **173**, 404 (2007).
4. L. Hao and P. Cheng, *J. Power Sources*, **186**, 104 (2009).
5. M.A. Van Doormaal and J.G. Pharoah, *Int. J. Numer. Meth. Fluids*, **59**, 75 (2009).
6. A. Nabovati, E. W. Llewelling and A. C. M. Sousa, *Composites: Part A*, **40**, 860 (2009).
7. P. P. Mukherjee, Q. Kang and C. Y. Wang, *Energy Environ. Sci*., **4**, 346 (2011).
8. P. Rama, Y. Liu, R. Chen, H. Ostadi, K. Jiang, X. Zhang, Y. Gao, P. Grassini and D. Brivio, *Int. J. Numer. Meth. Fluids*, **67**, 518 (2010).
9. P. Rama, Y. Liu, R. Chen, H. Ostadi, K. Jiang, Y. Gao, X. Zhang, D. Brivio and P. Grassini, *Fuel Cells*, **11**, 274 (2011).
10. P. Rama, Y. Liu, R. Chen, H. Ostadi, K. Jiang, X. Zhang, R. Fisher and M. Jeschke, *J. Fuel Cell Sci. Technol.*, **7**, 031015 (2010).
11. Y. Gao, X. X. Zhang, P. Rama, Y. Liu, R. Chen, H. Ostadi and K. Jiang, *Trans. Porous Media*, **92**, 457 (2012).
12. H. Ostadi, P. Rama, Y. Liu, R. Chen, X. Zhang and K. Jiang, *Microelectron. Eng.*, **87**, 1640 (2010).
13. H. Ostadi, P. Rama, Y. Liu, R. Chen, X. X. Zhang and K. Jiang, *Chem. Eng. Sci.*, **65**, 2213 (2010).
14. H. Ostadi, P. Rama, Y. Liu, R. Chen, X. X. Zhang and K. Jiang, *J. Membr. Sci.*, **351**, 69 (2010).